Chinese Journal of Catalysis 42 (2021) 2094–2104

available at www.sciencedirect.com

journal homepage: www.sciencedirect.com/journal/chinese-journal-of-catalysis

Review

Electrocatalysts development for hydrogen oxidation reaction in alkaline media: From mechanism understanding to materials design

Yang Qiu [a], Xiaohong Xie [a], Wenzhen Li [b,c,#], Yuyan Shao [a,*]

[a] *Pacific Northwest National Laboratory, Richland, Washington 99352, USA*
[b] *Department of Chemical & Biological Engineering, Iowa State University, Ames, IA, USA*
[c] *DOE's Ames Laboratory, Ames, IA, USA*

ARTICLE INFO

Article history:
Received 18 January 2021
Accepted 7 April 2021
Available online 10 September 2021

Keywords:
Hydrogen oxidation reaction
Alkaline electrolyte
Fuel cell
Electrocatalyst
Electrocatalysis
Hydrogen and hydroxide binding energy

ABSTRACT

Anion exchange membrane (AEM) fuel cells have gained great attention partially due to the advantage of using non-precious metal as catalysts. However, the reaction kinetics of hydrogen oxidation reaction (HOR) is two orders of magnitude slower in alkaline systems than in acid. To understand the slower kinetics of HOR in base, two major theories have been proposed, such as (1) pH dependent hydrogen binding energy as a major descriptor for HOR; and (2) bifunctional theory based on the contributions of both hydrogen and hydroxide adsorption for HOR in alkaline electrolyte. Here, we discuss the possible HOR mechanisms in alkaline electrolytes with the corresponding change in their Tafel behavior. Apart from the traditional Tafel-Volmer and Heyrovsky-Volmer HOR mechanisms, the recently proposed hydroxide adsorption step is also discussed to illustrate the difference in HOR mechanisms in acid and base. We further summarize the representative works of alkaline HOR catalyst design (e.g., precious metals, alloy, intermetallic materials, Ni-based alloys, carbides, nitrides, etc.), and briefly describe their fundamental HOR reaction mechanism to emphasize the difference in elementary reaction steps in alkaline medium. The strategy of strengthening local interaction that facilitates both H_2 desorption and H_{ads} + OH_{ads} recombination is finally proposed for future HOR catalyst design in alkaline environment.

1. Introduction

Hydrogen as a critical and indispensable element plays a significant role in a secure, clean and sustainable energy system [1,2]. Operating on H_2 (anode) and O_2/Air (cathode) feeds, fuel cells enable a high energy conversion efficiency and lower emissions [3]. Therefore, great efforts have been devoted for the development of fuel cells in both acidic and alkaline media [4]. As compared to proton exchange membrane (PEM) fuel cells, anion exchange membrane (AEM) fuel cells provide the benefits of using Pt group metal-free (PGM-free) catalysts for both hydrogen oxidation reaction (HOR) and oxygen reduction reaction (ORR) [5–13]. For reaction kinetics in AEM fuel cells, oxygen reduction reaction (ORR) on cathode exhibits an at least five orders of magnitude lower exchange current density ($i_{0,s}$) than hydrogen oxidation reaction (HOR) on anode over precious metals, such as Pt [14–18]. Accordingly, ORR has gained much higher attentions compared to the HOR from the catalyst design and development perspective due to the sluggish kinetics. However, it is important to note that considering Pt catalyst, the intrinsic kinetics of HOR is two orders of magnitude slower in alkaline electrolytes than in acidic environment,

* Corresponding author. E-mail: yuyan.shao@pnnl.gov
# Corresponding author. E-mail: wzli@iastate.edu
DOI: 10.1016/S1872-2067(21)64088-3 | http://www.sciencedirect.com/journal/chinese-journal-of-catalysis | Chin. J. Catal., Vol. 42, No. 12, December 2021

which could largely reduce the overall energy efficiency of AEM fuel cells [16–18]. For example, Gasteiger and co-workers reported the HOR $i_{0,s}$ of 120 mA cm^{-2}_{Pt} at 40 °C and 470 to 600 mA cm^{-2}_{Pt} at 80 °C over Pt/C in PEM fuel cells [19,20]. In contrast, Sheng *et al*. [18] reported the HOR $i_{0,s}$ of 0.69 and 0.57 mA cm^{-2}_{Pt} in 0.1 M NaOH at 21 °C over polycrystalline (pc) Pt and Pt/C, respectively. Rheinländer *et al*. [16] also demonstrated the HOR $i_{0,s}$ of 0.55 mA cm^{-2}_{Pt} from Pt(pc) in 0.1 M NaOH at 20 °C. Similar HOR activity decreases from acid to base was also observed in case of other PGMs, such as Pd (5.4 to 0.06 mA cm^{-2}_{Pd} at 40 °C), Ir (48 to 0.4 mA cm^{-2}_{Ir} at 40 °C), etc. [15,20,21]. Owing to this relatively slow HOR kinetics in alkaline electrolyte, a large HOR overpotential of 130 to 150 mV is expected to operate anion exchange membrane fuel cell (AEMFC) with a current density of 1.5 A cm^{-2}_{geo} at 80 °C. To circumvent this issue, often a higher Pt loading is required [12,18].

To understand the HOR kinetics in alkaline medium, different interpretations have been proposed. Yan's group reported the hydrogen binding energy (HBE) (i.e., derived from the differential Gibbs free energy of hydrogen adsorption, ΔG_{H^*}) is the sole descriptor that can control the HOR and hydrogen evolution reaction (HER) activity in alkaline environment in presence of different monometallic catalysts [21–23]. They found that most metals have stronger hydrogen binding in base than in acid, and a volcano-typed relationship between hydrogen binding energy and $i_{0,s}$ of HOR/HER also can be established [24–26]. Sheng *et al*. [22] further proposed a pH-dependent HBE theory by correlating the HBE with hydrogen underpotential deposition (H_{upd}) peak position measured in different pH buffer solutions, and found that hydrogen adsorption strength monotonically increases with pH. However, Koper and co-workers pointed out that H_{upd} peaks position could be affected by the adsorption of both hydrogen and oxygenated species [27,28]. Janik and co-workers also reported that the cation-hydroxyl co-adsorption contributes to pH dependence of HBE on Pt electrode, and changing pH with cations varying in the near surface region can change very little on hydrogen and metal interaction [29,30]. Based on these studies, Yan and Xu groups re-defined the HBE as the apparent hydrogen binding energy (HBE_{app}) which involves both HBE and water adsorption energy (i.e., $\Delta G_{H^*,app} = \Delta G_{H^*} - \Delta G_{H2O^*}$) [31,32]. They demonstrated that the intrinsic HBE is pH independent, while water adsorption strength is weakened with increasing pH (i.e., the value of ΔG_{H2O^*} increases). Consequently, the value of HBE_{app} (i.e., $\Delta G_{H^*,app}$) decreases as pH increasing, leading to the shift in H_{upd} peak position along with the change in pH. On the other hand, a bifunctional mechanism was proposed by Markovic and co-workers to explain the slower HOR kinetics at high pH. They proposed that both oxophilicity of catalyst and optimal HBE benefit HOR in alkaline electrolyte, as evidenced by higher HOR activity on oxophilic Ru and PtRu catalysts than Pt in alkaline solution [33–35]. This bifunctional mechanism pertaining to the HOR in alkaline medium has recently been studied. Correspondingly, HOR mechanism based on OH^- adsorption and consequent 3D volcano-type relationship was recently proposed as a guidance for HOR catalysts design and development in alkaline media [36–38].

The objective of the present review article is to discuss the recent progress in alkaline HOR with a special emphasis on reaction mechanism. The design principle and the corresponding electrocatalyst development based on sole HBE and bifunctional theory is highlighted. We start with a brief description of fundamental HOR reaction mechanism to emphasize the difference in elementary reaction steps in alkaline medium. Then, we summarize the representative alkaline HOR catalysts, including both precious and non-precious catalysts. Finally, we provide perspectives for future alkaline HOR catalyst design and development according to the improvement of interaction between two factors that facilitate H_2 dissociation and recombination of adsorbed hydrogen and hydroxide, respectively.

2. Kinetic analysis and mechanisms of HOR

In acid, HOR can be simply described by two out of three elementary steps involving hydrogen species only (i.e., H_2, H_{ads}, H^+), which are dissociative adsorption of H_2 without electron transfer (Tafel step), or with one electron transfer (Heyrovsky step), and the desorption of adsorbed hydrogen (H_{ads}) [18,39].

The elementary steps of HOR reaction in acid:

$$\text{Tafel:} \quad H_2 + 2^* \leftrightarrow 2H_{ads} \tag{1}$$

$$\text{Heyrovsky:} \quad H_2 + ^* \leftrightarrow H_{ads} + H^+ + e^- \tag{2}$$

$$\text{Volmer:} \quad H_{ads} \leftrightarrow H^+ + ^* + e^- \tag{3}$$

In base, the hydroxide ion participates into the reaction, and Heyrovsky and Volmer steps can be written as follows [12,18].

The elementary steps of HOR reaction in base:

$$\text{Tafel:} \quad H_2 + 2^* \leftrightarrow 2H_{ads} \tag{4}$$

$$\text{Heyrovsky:} \quad H_2 + OH^- + ^* \leftrightarrow H_{ads} + H_2O + e^- \tag{5}$$

$$\text{Volmer:} \quad H_{ads} + OH^- \leftrightarrow H_2O + ^* + e^- \tag{6}$$

Apart from the well-defined HOR mechanisms, Mukerjee's group further specified the hydroxide adsorption and subsequent H_2O formation in alkaline electrolyte [12,40,41]. They proposed that the negative charge on electrode surface with high activation energy barrier of hydroxide anion adsorption (OH^-) for Pt could prevent the directly OH^- adsorption on monometallic metals but form a quasi-specific interaction ($Pt\text{-}H_{ads}\cdots OH_{q\text{-}ad}$) between H_{ads} and OH^- (Scheme 1 in Fig. 1). In the case of bimetallic catalysts, e.g., PtRu, it enables the formation of $Ru\text{-}H_{upd}\cdots OH_{q\text{-}ad}$ *via* one electron transfer, followed by migration of $OH_{q\text{-}ad}$ to react with neighboring $Pt\text{-}H_{ads}$ (Scheme 2 in Fig. 1). When non-noble transition metals (e.g., Nb, Ni, Cu, etc.) were incorporated and formed an alloy with Pt, a thin layer of non-noble metal oxide/hydroxide could be generated. The OH^- could be adsorbed on adjacent alloying element in the fashion of $NbO_x(OH_y)/Cu\text{-}OH_{ad}/Ni\text{-}OH_{ad}$, and reacts with neighboring $Pt\text{-}H_{ads}$ following the Scheme 3 in Fig. 1 [12,40,41]. Similar mechanism of Scheme 3 was demonstrated on Pt(553) electrode with high coverage of Mo, Re, and Ru by McCrum *et al*. [37]. They proposed that the RDS of HER/HOR could be the adsorbed hydroxide (OH_{ads}) desorption step for HER and H_{ads}+OH_{ads} recombination for HOR [37]. As a result, a new HOR mechanism with OH^- adsorption step in base was rewritten as Eqs. (7) to (9).

The elementary steps of HOR reaction with hydroxide adsorption/desorption in base:

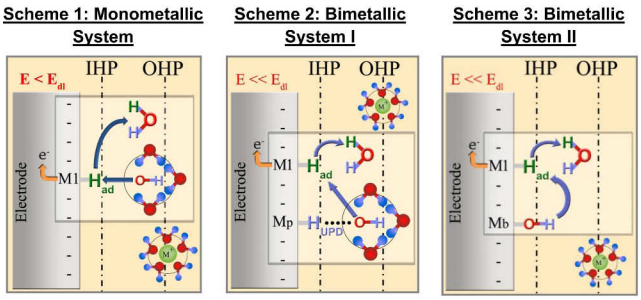

Fig. 1. Relationship between HOR electrocatalysis and electrochemical double-layer structure. Generic mechanistic reaction schemes for HOR in dilute alkaline electrolytes on mono and bi-metallic catalyst systems. M1 represents a metal site capable of dissociative adsorption of molecular hydrogen. In scheme 2, alloy element Mp represents a precious metal site capable of forming H_{upd} in alkaline electrolyte. In scheme 3, alloy element Mb represents a base-metal site passivated with adsorbed (hydr)oxide species in dilute alkaline electrolytes. (Reproduced from Ref. [40] with permission from Elsevier. Copyright (2017)).

Tafel: $H_2 + 2* \leftrightarrow 2H_{ads}$ (7)

OH^- adsorption: $OH^- + * \leftrightarrow OH_{ads} + e^-$ (8)

H_{ads} and OH_{ads} recombination: $H_{ads} + OH_{ads} \leftrightarrow H_2O + 2*$ (9)

Following two out of three elementary steps of Tafel, Heyrovsky, and Volmer, HOR has four possible reaction mechanisms, including Tafel-Volmer(RDS), Tafel(RDS)-Volmer, Heyrovsky-Volmer(RDS), and Heyrovsky(RDS)-Volmer. As shown in Tables 1 and Fig. S1, when HOR/HER follows Tafel-Volmer(RDS) mechanism, the same ideal Tafel slopes of ~118 mV dec^{-1} are determined from both HOR and HER in universal pH, resulting in a symmetrical Tafel plot. However, a ~29 mV dec^{-1} Tafel slope was commonly reported previously on Pt and Pt-based HOR catalysts in acid by using RDE technique [39,42]. However, this lower Tafel slope (~29 mV dec^{-1}) is originated from the H_2 transfer limit instead of fast HOR kinetics [18]. To investigate the HOR mechanism in acid, H_2-pump system with higher H_2 supplying rate was developed, and a much higher Tafel slope of ~118 mV dec^{-1} was obtained on PGM catalysts, indicating their Tafel-Volmer(RDS) mechanism for HOR/HER [16,20]. In contrast, the two orders of magnitude slower HOR kinetics in base allows the intrinsic Tafel slope measurement by using RDE technique. For PGM HOR catalysts, very similar Tafel slopes ranging from 109 to 116 mV dec^{-1} were determined from Pt(pc), Pd/C, and Ir/C [21,43,44]. As a result, it can be predicted that HOR/HER follows the same mechanism of Tafel-Volmer(RDS) in both acidic and alkaline environment over most precious metals (e.g., Pt, Pd, Ir, etc.).

For the Tafel-Volmer mechanism with Tafel step as the RDS, HER possesses a Tafel slope of ~29 mV dec^{-1} in both acid and base. However, The ideal current-potential relationship of HOR through Tafel(RDS)-Volmer is still in debate. Since the Tafel step is chemical reaction in the absence of electron transfer, the HOR current should be independent of overpotential, which has been demonstrated by Shinagawa *et al.* [45]. They incorporated hydrogen partial pressure (p_{H2}) into HOR kinetics expression, and found that HOR current was proportional to p_{H2} only by assuming negligible hydrogen coverage on catalysts surface [45]. In contrast, Krischer *et al.* [46] reported the HOR Tafel slope of ~30 mV dec^{-1} by assuming quasi-equilibrium of Volmer step in Tafel(RDS)-Volmer mechanism in both acid and alkaline. In practical, Heyrovsky-Volmer(RDS) could couple with Tafel(RDS)-Volmer mechanism, leading to a larger Tafel slope than that of ~29 mV dec^{-1}.

When HOR/HER follows Heyrovsky-Volmer mechanisms, an asymmetrical Tafel plot could be obtained. For example, HOR possesses a Tafel slope of ~118 mV dec^{-1}, while HER shows ~39 mV dec^{-1} Tafel slope with Heyrovsky step as the RDS. The Tafel slopes are reversed when Volmer step becomes RDS (TS_{HOR} = ~39 mV dec^{-1}, TS_{HER} = ~118 mV dec^{-1}). It should be noted that same Tafel slopes of ~118 mV dec^{-1} could be obtained from HOR with Tafel-Volmer(RDS) and Heyrovsky(RDS)-Volmer mechanisms, and from HER with Tafel-Volmer(RDS) and Heyrovsky-Volmer(RDS) mechanisms. Therefore, the collection of both HOR and HER Tafel plots is highly recommended for reaction mechanism determination. In addition, a larger overpotential of $|\eta|$ > 118 mV (at 25 °C, α = 0.5) is required to minimize backward reaction interference (i.e., backward reaction rate <1 %) for Tafel slope measurement [47,48]. When HOR kinetics is too fast on the specific catalyst, a smaller overpotential of 118 mV > $|\eta|$ > 59 mV is acceptable to avoid reaching mass-transfer limiting current [49].

Table 1
Tafel slope and kinetic expressions for HOR.

HOR mechanism	Tafel slope at 25 °C	Note
Heyrovsky-Volmer(RDS)	2.303RT/[(2–α)F] = ~39 mV dec^{-1}	θ_H < 0.4 (low η_{Vol}) TS = 39 θ_H > 0.6 (high η_{Vol}) TS = 118 (close to Heyrovsky-RDS)
Tafel-Volmer(RDS)	2.303RT/[(1–α)F] = ~118 mV dec^{-1}	θ_H is govern by P_{H2} Reaction rate is governed by both η and θ_H (P_{H2})
Heyrovsky(RDS)-Volmer	2.303RT/[(1–α)F] = ~118 mV dec^{-1}	H_{ads} consumes rapidly ($\theta_H \approx 0$); fast Volmer step
Tafel(RDS)-Volmer*	2.303RT/2F = ~29 mV dec^{-1}	H_{ads} consumes rapidly ($\theta_H \approx 0$); fast Volmer step Reaction rate could be independent to η ($I = nFAk^{o}_{T}P_{H2}$)

*α is the charge transfer coefficient of HER, α = 0.5 (i.e., 1–α = 0.5 for HOR), θ_H is hydrogen coverage, F is faradaic constant, A is surface area, k^{o}_{T} is rate constant, P_{H2} is hydrogen gas partial pressure; For HOR mechanism of Tafel(RDS)-Volmer, Krischer et al. reported the HOR Tafel slope of ~29 mV dec^{-1} by assuming quasi-equilibrium of Volmer step in Tafel(RDS)-Volmer mechanism in both acid and alkaline [46], while Shinagawa et al. reported that HOR current should be proportional to P_{H2} only by assuming negligible hydrogen coverage on catalysts surface [45].

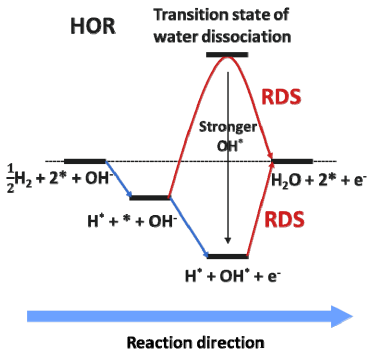

Fig. 2. Reaction energy diagram showing the complete reaction pathway with rate determining steps for hydrogen oxidation for a catalyst which has a hydroxide adsorption strength from weak to strong. Reproduced from Ref. [37] with the permission from Springer Nature. Copyright (2020).

For OH^- adsorption/desorption involved HOR/HER mechanism (Eqs. 7–9), McCrum *et al.* reported that the HER RDS could shift from water dissociation (Volmer step, Eq. 6 backward reaction) to OH_{ads} desorption (Eq. 7 backward reaction) when hydroxide adsorption strength changes from too weak to too strong on the Pt-based catalysts [37]. They demonstrated that both optimal adsorption of hydroxide (ΔG_{OH^*} = 0.15 to 0.25 eV) and hydrogen (ΔG_{H^*} = 0 eV) are required to promote the HER activity in alkaline electrolyte. Following the same investigation strategy, they found that HOR in alkaline electrolyte shares the same RDS of Volmer step (Eq.6 forward reaction) on the catalysts with too weak hydroxide adsorption strength (Fig. 2). However, the catalyst that binds OH^- too strong shows RDS as the recombination of H_{ads} + OH_{ads} during HOR (Eq. 9 forward reaction), which is different in case of HER whereas OH_{ads} desorption being RDS (Fig. S1). We considered the hydroxide binding energy (OHBE) reported in the literature by Nørskov *et al.* [50] as a reference to compare the hydroxide adsorption strength across different metals (Table 2).

Table 2
Calculated hydroxide binding energy (ΔE_{OH^*}) over the most close packed surface of different metals at a quarter monolayer coverage, data is cited from Ref. [50].

Metal	ΔE_{OH^*}/eV	Metal	ΔE_{OH^*}/eV	Metal	ΔE_{OH^*}/eV
Ag	0.72	Au	1.49	Co	−0.08
Cu	0.37	Fe	−0.88	Ir	0.63
Mo	−0.61	Ni	0.13	Pd	0.92
Pt	1.05	Rh	0.34	Ru	−0.01
W	−0.80				

3. Representative works of HOR catalyst design and development in alkaline environment

3.1. Precious metal-based HOR catalysts

Trasatti and Nørskov groups empirically correlated the $i_{0,s}$ of HOR/HER in acid with the hydrogen adsorption energies (derived from the differential Gibbs free energy of hydrogen adsorption, ΔG_{H^*}) of different monometallic catalysts, and found a volcano-shaped relation (Fig. 3(a)) [24,25]. Yan's group established a similar volcano-shaped relationship in base (Fig. 3(b)) between $i_{0,s}$ of HOR/HER and HBE_{app} (i.e., $\Delta G^0_{H^*,app} = \Delta G^0_{H^*} - \Delta G^0_{H2O^*}$), which has been considered as the most important guidance for HOR/HER catalysts design [21,31]. PGMs (e.g., Pt, Pd, Ir, Rh, etc.) feature the optimal HBE closed to volcano peak, thereby exhibiting higher HOR/HER activities than other non-precious metals that adsorb hydrogen either too strong or too weak [24,25,51]. To optimize HBE, the second element was introduced, and different material constructions were prepared, including surface alloy with monolayer coverage, core-shell structure, bulk alloy, etc. [42,52–58]. For example, Scofield *et al.* [58] prepared Pt-M alloy (M = Cu, Ru, Co, Fe, Au), and found that the alkaline HOR $i_{0,s}$ of Pt-M is enhanced by

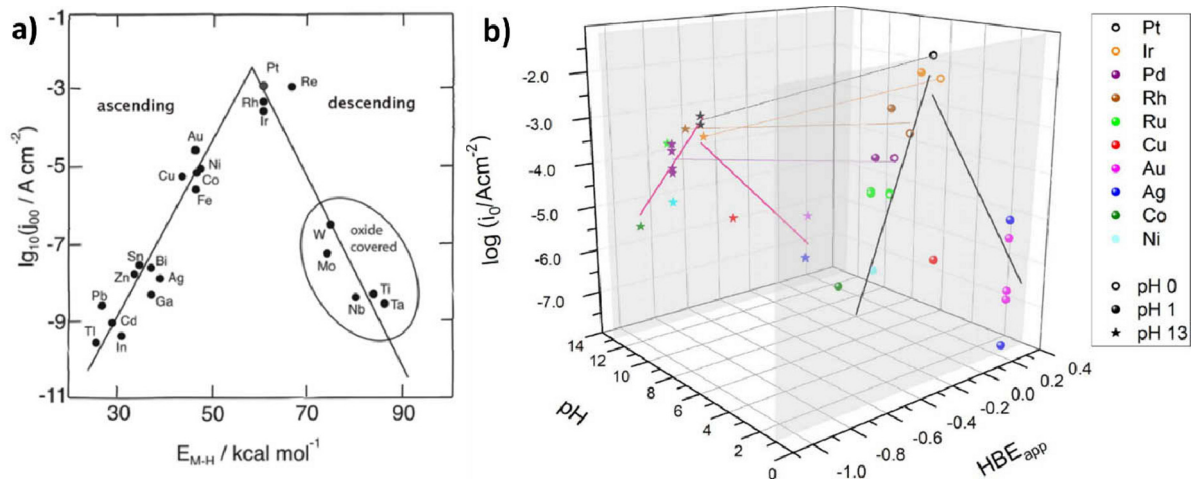

Fig. 3. (a) Trassati's volcano plot for the hydrogen evolution reaction in acid solutions. j_{00} (same to j_0) denotes the exchange current density, and E_{MH} is the energy of hydride formation. (Data is taken from Ref. [24]. Reproduced from Ref. [51] with the permission from Dr. Wolfgang Schmickler). (b) Schematic illustrating the research need to establish HBE_{app} as the descriptor for HOR/HER: (1) Measuring and/or calculating water adsorption energy of PGMs in different pHs; (2) Measuring and/or calculating water adsorption energy of metals on the weakly binding branch in different pHs; (3) Measuring HOR/HER activities on metals on the weakly binding branch. Exchange current density data represents the activity at 20 °C, and is from [18,20,25,32,57,70,71]. (Reproduced from Ref. [31] with open access).

weakened HBE, which can be well fitted into volcano relationship between $i_{0,s}$ and HBE. (Fig. 4(a)). Over the past decade, PtRu was commonly used as HOR catalyst in AEM fuel cells, featuring a higher activity (i.e., $i_{0,s}$ = 0.6 to 1.4 mA cm$^{-2}_{Pt}$ at 25 °C) than other Pt-M alloys (i.e., $i_{0,s}$ < 0.4 mA cm$^{-2}_{Pt}$ at 25 °C) [34,40,58–61]. The high activity of PtRu was initially interpreted to be the optimally weakened HBE by Ru incorporation. However, the higher oxophilicity associated with Ru was also invoked to benefit OH^- adsorption on PtRu surface, thereby, facilitating HOR in alkaline environment [34,62]. PtNi nanoparticles (NPs) ($i_{0,s}$ = 1.7 mA cm$^{-2}_{Pt}$ at 25 °C) and Pt coated Cu nanowires (NWs) ($i_{0,s}$ = ~2.0 mA cm$^{-2}_{Pt}$ at 25 °C) were also reported to exhibit remarkable HOR activities, which can be ascribed to their optimized HBE and desired oxophilicity [40,56,63].

Considering stronger hydrogen binding with Pd surface compared to Pt, weakening of HBE is more important to enhance HOR activity of Pd [54]. Pd-M bimetallic materials were more prepared by Pd atomic layer deposition on other metal substrates (e.g., Au, Pt, Rh, Ir, Ru, Re, etc.) to mitigate hydrogen diffusion interference issue [20,54]. However, the lower intrinsic HOR activity of Pd than Pt makes the Pd-based HOR catalysts less attractive than Pt-M [20,54,64]. To our best knowledge, Pd coated Cu NWs ($i_{0,s}$ = ~1.0 mA cm$^{-2}_{Pd}$ at 25°C) prepared by Alia *et al*. [57] was reported to be the most active catalyst among all Pd-based HOR catalysts in alkaline medium.

Despite the similar HBE and much lower cost of Ru than Pt (Fig. 4(b)) [65]. monometallic Ru was rarely reported as the HOR catalysts because of (1) its low passivation potential of ~0.3 V *vs*. a reversable hydrogen electrode (RHE) [66], and (2) its HOR performance sensitivity toward materials morphology and particle size [67,68]. Recently, Wei's group reported the lattice-confined Ru cluster on TiO_2 with Ru-Ti interface as the active site for HOR in base, which significantly improves the electrochemical stability up to 0.9 V *vs*. RHE [66]. Xue *et al*. [59] also reported a highly active HOR catalyst of Ru_7Ni_3/C in alkaline environment which outperforms to PtRu/C in both specific activity and mass activity at 50 mV overpotential (Ru_7Ni_3/C shows 3 and 5 times higher specific activity and mass activity respectively compared to PtRu/C). In addition, this Ru_7Ni_3/C was further tested as the anode catalyst in a H_2/O_2 AEMFC, and it exhibited a 1.3 times higher peak power density (peak power density = 2.03 W cm$^{-2}_{geo}$) than PtRu/C at 95 °C.

Markovic's group [33] formally proposed the bifunctional theory and demonstrated that the $Ni(OH)_2$ cluster decorated on Pt(111) could enhance the HOR activity of Pt(111) in alkaline electrolyte by improving the adsorption of reactive OH_{ads} (Fig. 5(a)). Consequently, the hydroxide adsorption was coined as another descriptor, to provide a guidelinefor alkaline HOR catalyst design and development. Koper's group [37] further developed this bifunctional theory and taken OH^- adsorption/desorption step into the consideration of HOR/HER mechanism investigation. By correlating the HBE and OHBE with HER rate in alkaline electrolyte, they clearly illustrated the desired HBE and OHBE for HER catalyst design (Fig. 5(b)), and the same strategy was applied for HOR mechanism analysis. When a catalyst binds OH^- too weak (volcano right side), the HOR activity in base is proportional to increased OH_{ads} binding strength (Fig. 5(c)). However, if the OH_{ads} binding strength moves to stronger OH_{ads} binding side (volcano left side of Fig. 5(c)), the optimal hydroxide adsorption energies could be different for HOR and HER. Further increasing OH_{ads} strength might improve the HER activity but hinder the rate of HOR in alkaline electrolyte as compared to monometallic Pt. This is mainly attributed to the larger energy barrier of H_{ads} + OH_{ads} recombination (RDS of HOR) than OH_{ads} desorption (RDS of HER) (Fig. 2). Therefore, the overall HOR rate could be lower than that of HER over the same bifunctional catalysts with strong OH_{ads}. Based on the understanding of bifunctional theory discussed herein, the HOR performance enhancement over

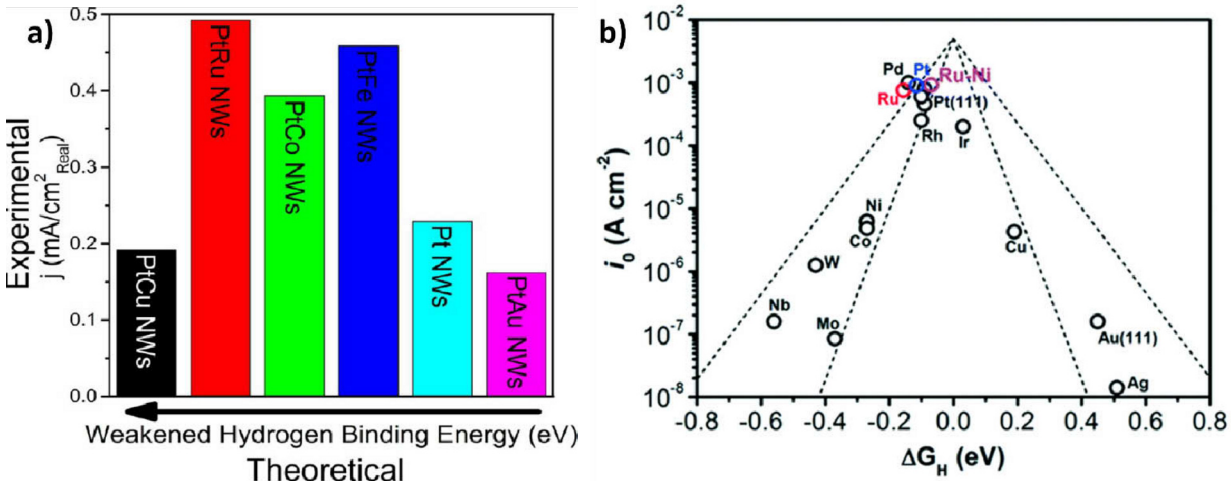

Fig. 4. (a) Bar graph highlighting experimental HOR exchange current densities as a function of the corresponding trend on the basis of calculated surface hydrogen binding energy (HBE) values for models of "near surface alloys" for Pt, Pt_7Ru_3, Pt_7Fe_3, Pt_7Co_3, Pt_7Cu_3, and Pt_7Au_3 NWs, respectively. The trend shown for the theoretical HBE values was based upon the data presented in Ref. [72]. (Figure is reproduced from Ref. [58] with the permission from American Chemical Society. Copyright (2016)). (b) The volcano plot of the experimentally measured exchange current density versus the adsorption hydrogen free energy of Ru-Ni (magenta), Ru (red) and Pt (blue) calculated by DFT in this study where the ΔG_H of Ru and Pt were taken from the value most close to 0, and common metal catalysts. (Reproduced from Ref. [65] with the permission from Royal Society of Chemistry. Copyright (2020)).

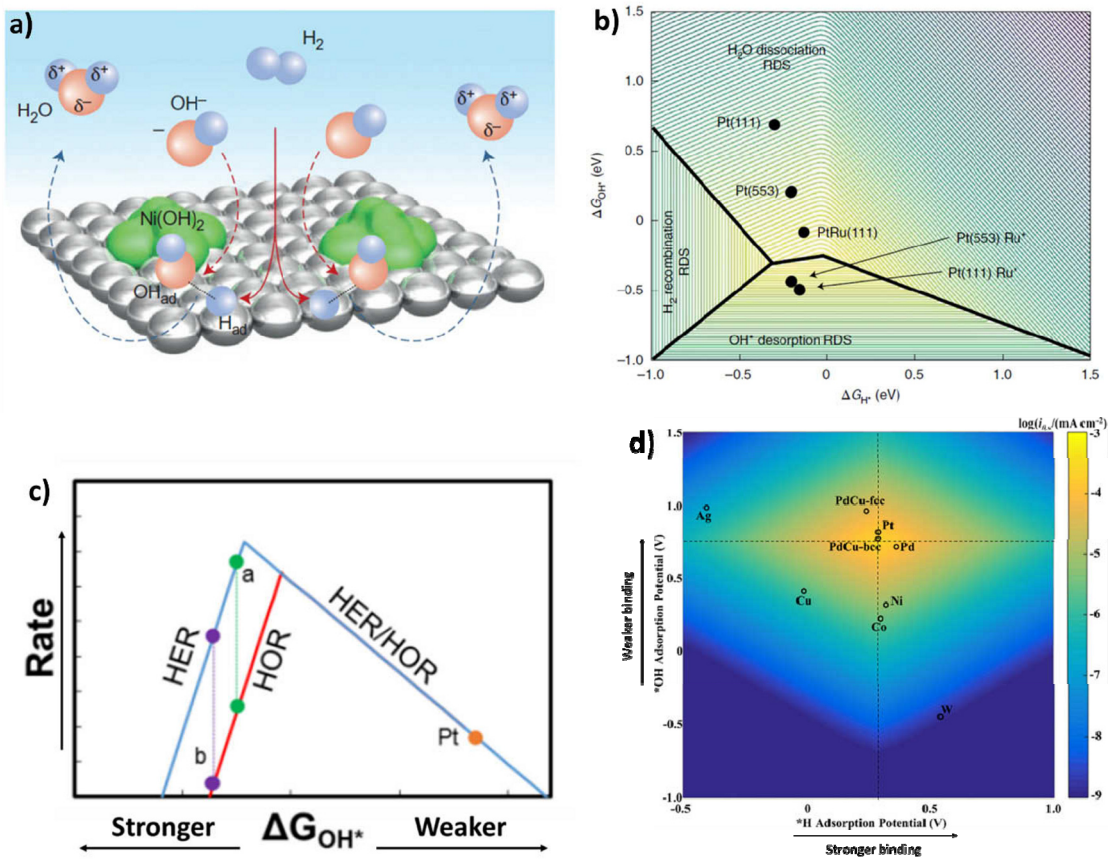

Fig. 5. (a) Schematic representation of the HOR on $Ni(OH)_2$/Pt(111), $Ni(OH)_2$ provides the active sites for adsorption of reactive OH_{ads}, and Pt provides the active sites for dissociative adsorption of H_2 and production of H_{ads}, which then react with reactive OH_{ads}. (Reproduced from Ref. [33] with the permission from Springer Nature. Copyright (2013)). (b) 3D HER activity volcano for catalyst design. Logarithm of the rate of hydrogen evolution (contours) as a function of hydrogen binding energy and hydroxide binding energy. The water dissociation rate was derived from the binding energies and kinetics on (211) surfaces calculated previously and modified to reference solution-phase hydroxide as the product of water dissociation and then extrapolated to 0 V_{RHE} and to reproduce the barriers calculated here for water dissociation on Pt(111) and Pt(553) (which include the effects of solvation and alkali cation). Black circles correspond to DFT-calculated hydrogen and hydroxide adsorption energies on Pt(111), Pt(553), Ru* adsorbed at the step of Pt(553), a PtRu(111) alloy and Ru* clusters on Pt(111). (c) Rate of the HER or the HOR as a function of the free energy of adsorption of hydroxide. (Figure b and c are reproduced from Ref. [37] with the permission from Springer Nature. Copyright (2020)). (d) Experimentally measured exchange current density, $\log(i_{0,s})$, for hydrogen oxidation in base over different metals plotted with calculated H and OH adsorption potentials. The two dashed lines represent the optimal *H adsorption potential (~0.28 V) and the optimal *OH adsorption potential (~0.75 V), respectively. (Reproduced from Ref. [36] with the permission from American Chemical Society. Copyright (2018)).

PtRu(111) [37], PtNb [40], RuNi [59], IrPdRu [69], etc. can be well explained by both weakened HBE and enhanced hydroxide adsorption strength. Qiu *et al.* [36] reported a 3D correlation between HBE, OHBE and HOR activity (i.e., $i_{0,s}$) in alkaline media (Fig. 5(d)). They found that the crystalline structure transformation from fcc to bcc crystalline structure can strengthen the OH_{ads} binding of PdCu, and the incorporated Cu is able to weaken the HBE of Pd. As a result, a 1.2 times higher HOR activity than Pt was obtained from bcc-phased PdCu, and this work opened a new route to develop efficient alkaline HOR catalysts from the perspective of crystalline structure transformation [36].

3.2. *Non-precious HOR catalysts*

One of the most often cited advantages of AEM fuel cells is its independence of precious metals [5,8]. Though, considerable effort has been made at the cathode side for oxygen reduction [73–77], however, very limited numbers of PGM-free HOR catalysts in alkaline electrolytes have been reported which could be attributed to their lower oxidation potential compared to the Pt group metal. Ni features a comparable HOR activity ($i_{0,s}$ = 0.008 mA cm^{-2}_{Ni}) compared to its other congeners (e.g., $i_{0,s}$ = 0.003 mA cm^{-2}_{Co} for Co, 0.001 mA cm^{-2}_{Cu} for Cu) [21], and has been extensively studied [23,78–90]. As compared to PGM, Ni has stronger hydroxide binding strength than Pt, Pd, and Ir, which could facilitate the HOR kinetics in base. However, the much stronger HBE of Ni than Pt (Fig. 3) becomes the main challenge for HOR activity improvement. Two major strategies were applied to weaken HBE of Ni, including (1) incorporating the second element to form Ni-M alloy or nitride (M = Cu, Mo, N, etc.) with weakened HBE [23,80–82,85,87,91]; and (2) modifying the supporting materials of Ni to weaken the HBE of interfacial Ni sites [78,79,86]. Sheng *et al.* [23] reported that Co

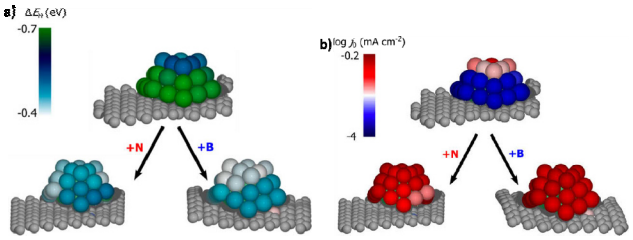

Fig. 6. (a) Heat map of the local hydrogen adsorption energy for Ni/graphene (top), Ni/*N*-graphene (bottom left), and Ni/B-graphene (bottom right). (b) Heat map of the local HOR/HER exchange current density for Ni/graphene (top), Ni/*N*-graphene (bottom left), and Ni/B-graphene (bottom right). (Reproduced from Ref. [78] with the permission from American Chemical Society. Copyright (2019)).

and Mo incorporation in Ni is able to weaken HBE of Ni from –0.51 to –0.43 eV, thereby promoting its HOR activity by one fold ($i_{0,s}$ = 0.015 mA cm$^{-2}_{metal}$). Savinov's group incorporated Cu into Ni (Ni_xCu_y alloy), and found that the 5 at% Cu incorporation achieved the highest HOR activity of $i_{0,s}$ = 0.014 mA cm$^{-2}_{Ni}$, which is about 2 times higher than that of pristine Ni in alkaline media [85,91]. In addition to the bimetallic catalysts, Ni nitride was also demonstrated to be more active than Ni for alkaline HOR. Sun and Hu groups demonstrated that the Ni_3N/Ni interface (ΔG_{H^*} = 0.01 eV) possesses the lower energy barrier of H_{ads} than pure Ni (ΔG_{H^*} = –0.30 eV) and Ni_3N (ΔG_{H^*} = –0.57 eV) [81,82]. Therefore, Ni_3N/Ni is expected to exhibit higher HOR activity. On the other hand, Yan and Vlachos *et al.* demonstrated that the HBE of the metal sites near the nanoparticle-support interface is strongly affected by supporting materials (Fig. 6(a)) [78]. Their DFT modeling and experimental results clearly illustrated that the N-doped or B-doped graphene apparently decreases the HBE of Ni atoms in the nanoparticle-support interface. As a result, the Ni/N-graphene and Ni/B-graphene exhibited a higher $i_{0,s}$ than Ni/graphene and Ni(111) particles (Fig. 6(b)). In addition, Yang *et al.* [21] found that S-doped carbon (SC) supporting material shows even lower energy barrier of hydrogen adsorption on Ni (ΔG_{H^*} = ~0 eV). Consequently, Ni/SC ($i_{0,s}$ = 0.04 mA cm$^{-2}_{Ni}$) outperformed to Ni/NC, Ni/BC, and Ni/C, and exhibited a 4 times higher $i_{0,s}$ than Ni/C ($i_{0,s}$ = 0.01 mA cm$^{-2}_{Ni}$). The HOR performance over different electrocatalysts in alkaline environment were summarized in Table 3.

4. Summary and Future perspectives

HOR kinetics in base is two orders of magnitude slower than that in acid, which makes HOR catalyst development an important research topic for AEM fuel cells. To develop highly active and cost-effective HOR catalysts in alkaline electrolytes, HOR mechanisms have been extensively studied by both experimental and computational approaches. In contrast to acid medium, which only involves hydrogen atoms, both water and hydroxide species are involved in base. Therefore, both HBE and OHBE are considered as the descriptor to regulate HOR activity in base. Over the past decade, the alkaline HOR catalyst development was guided from sole HBE optimization to bifunctional theory which considered the optimization of both HBE and OHBE (Fig. 7). Recently, more detailed mechanistic model has been proposed to analyze the change in RDS change with catalysts that binds both hydrogen and hydroxide either too strong or too weak. Pt and PGMs (i.g., Pd, Rh, Ir, Ru) feature stronger HBE than other non-precious metals (e.g., W, Ni,.Co, Nb, etc.), thus, have been extensively developed as promising HOR catalysts in base. PtRu was reported as the most active catalyst among all Pt-based HOR catalyst in base, which can be attributed to its optimally weakened HBE and enhanced oxophilicity (i.e., stronger hydroxide adsorption strength). Further mechanistic proposals are also provided to understand sluggish HOR in alkaline, including cation and ligand co-adsorption effect, potential of zero charge effect, etc (Fig. 7). We summarized the representative alkaline HOR catalysts which exhibited remarkable HOR activity and durability, including PtRu, Ru_7Ni_3, PdCu, etc. On the other hand, the non-precious HOR catalyst development remains a challenge because of the lower antioxidation properties of non-precious metals than precious metals. Ni has attracted the most attention due to its comparable HOR activity to that of noble metals in alkaline electrolytes. Despite the desired oxophilicity, modification of Ni catalyst is required to weaken its strong hydrogen binding strength. By incorporating the second element to form Ni-M alloy or nitride, the weakened HBE significantly benefits higher HOR performance in alkaline media. In addition, the heteroatom-doped supporting materials was also demonstrated to regulate the HBE of metal sites near the nanoparticle-support interface.

Built on the success of alkaline HOR catalyst development, mechanism understanding and materials innovation in the past decade (Fig. 7), further development can be made in the following aspects. The key aspect is to tune the local interaction such a way that facilitate both H_2 desorption and H_{ads} + OH_{ads} recombination, respectively. For example, intermetallic materials with highly ordered M_1-M_2 sites (M_1 for H_{ads}; M_2 for OH_{ads}) are promising to show a higher HOR activity than disordered alloys and bimetallic composites. Although many precious metal-based intermetallic materials were applied for HOR previously [36,57,93–95], non-precious metal-based intermetallic HOR catalysts were rarely reported. Non-precious metals generally feature stronger hydrogen adsorption strength (e.g., Ni, Fe, Co, etc.) than precious metals (e.g., Pt, Pd, Ru, etc.), thus, the second element is required to mainly tune the HBE of primary metal catalyst. In addition, small particle is preferred to enlarge the amount of HOR site from intermetallic materials and supporting material interface. The HBE of few layers intermetallic material is expected to be further optimized by supporting materials (e.g., heteroatom-doped carbon supporting materials), resulting in the alkaline HOR catalyst with an HBE more closed to volcano peak. Furthermore, the higher oxophilicity of non-precious metals could benefit their HOR activity in alkaline electrolyte. On the other hand, metal-metal oxide (or hydroxide) junction with M_1-O-M_2 interfacial site was expected to improve the recombination of H_{ads} + OH_{ads} for HOR activity promotion in base. We are finally targeting on the single atom-leveled electrocatalysts which is expected to significantly decrease catalysts cost with high activity. These strategies are applicable for HER catalyst design in alkaline media too.

Table 3
Summary of the HOR performance over representative electrocatalysts in alkaline electrolyte.

Catalyst	Reaction conditions			HOR performance			Ref.
	Electrolyte	Temperature (°C)	Loading (μg cm^{-2})	η to achieve i_l (mV *vs.* RHE)	Exchange current density (mA cm^{-2})	Tafel slope (mV dec^{-1})	
Pt(pc)	0.1 M KOH	21 ± 1.5	RDE	250–300	0.69 ± 0.03	109	[18]
Pt/C	0.1 M KOH	21 ± 1.5	7.0	~300	0.57 ± 0.07	—	[18]
Pt/C	0.1 M NaOH	40 ± 0.0	3.0	—	1.0 ± 0.01	—	[15]
Pt/Cu NW	0.1 M KOH	23 ± 3.0	16.0 (Pt)	~100	2.1 (Pt)	—	[56]
$Pt_{0.8}Ru_{0.2}$/C	0.1 M KOH	23 ± 3.0	7.09 (PtRu)	~140	1.42 (Pt)	35	[60]
PtRu/C	0.1 M KOH	23 ± 3.0	3.8 (PtRu)	~90	0.7 (Pt)	—	[34]
PtFe	0.1 M KOH	23 ± 3.0	8.0 (Pt)	>250	0.459 (Pt)	43.3	[58]
PtCo	0.1 M KOH	23 ± 3.0	8.0 (Pt)	>250	0.394 (Pt)	45.7	[58]
PtAu	0.1 M KOH	23 ± 3.0	8.0 (Pt)	—	0.162 (Pt)	49.6	[58]
Acid-PtNi/C	0.1 M KOH	23 ± 3.0	10.0 (Pt)	~250	1.89 ± 0.09 (Pt)	—	[63]
Pd/C	0.1 M NaOH	40 ± 0.0	16.0	—	0.06 ± 0.02	—	[15]
Pd/C-500C	0.1 M KOH	20 ± 0.0	20	~350	0.122 ± 0.005	108	[44]
Pd/Cu NW	0.1 M KOH	23 ± 3.0	12.5	>200	1.01 (Pd)	—	[57]
$Pd_{0.8}Ru_{0.2}$/C	0.1 M KOH	23 ± 3.0	7.06 (PdRu)	~375	0.148 (Pd)	219	[60]
Pd/C-CeO_2	0.1 M KOH	23 ± 3.0	6.5 (Pd)	—	0.089	100	[64]
Ir/C	0.1 M NaOH	40 ± 0.0	8.0	—	0.37 ± 0.12	—	[15]
Ir/C	0.1 M KOH	20 ± 0.0		~250	0.21 ± 0.02	116	[43]
Ir_9Ru_1/C	0.1 M KOH	23 ± 3.0	3.5 (IrRu)	~110	0.9 (IrRu)	—	[69]
$Ir_3Pd_1Ru_6$/C	0.1 M KOH	23 ± 3.0	3.5 (IrPdRu)	~100	0.6 (IrPdRu)	—	[69]
Ru/C	0.1 M KOH	25 ± 0.0	10.0	~120	0.064	—	[92]
Ru_1@Pt_1(2 ML)	1.0 M KOH	23 ± 0.0	~3.0	—	1.5 (Pt)	—	[55]
$Ru7Ni_3$/C	0.1 M KOH	23 ± 0.0	3.9 (Ru)	~100	1.09	—	[59]
CoNiMo	0.1 M KOH	20 ± 0.0	—	—	0.015 ± 0.009	—	[23]
Ni_1Cu_1/C	0.1 M KOH	25 ± 0.0	25 (NiCu)	—	0.0145	—	[85]
Ni/Graphene	0.1 M KOH	23 ± 3.0	250 (Ni)	—	0.030	—	[79]
Ni/N-CNT	0.1 M KOH	23 ± 3.0	250 (Ni)	—	0.028	—	[79]
Ni1@$(h\text{-}BN)_1$/C	0.1 M NaOH	23 ± 3.0	250 (Ni)	—	0.023	—	[86]
NiMo/KB	0.1 M KOH	25 ± 0.0	100 (w/C)	—	0.027 ± 0.002	—	[87]
WNi_4	0.1 M KOH	23 ± 3.0	500 (WNi)	~90	0.068	—	[89]
$MoNi_4$	0.1 M KOH	23 ± 3.0	500 (MoNi)	~80	0.065	—	[89]
Ni/SC	0.1 M KOH	23 ± 3.0	50 (w/C)	—	0.04	—	[83]

*(w/C) means with carbon.

Acknowledgments

This work was financially supported by the U.S. Department of Energy's (DOE), Energy Efficiency and Renewable Energy, Hydrogen and Fuel Cell Technologies Office (DOE-EERE-HFTO). We gratefully acknowledge Udishnu Sanyal and Litao Yan and at PNNL for their help with the discussions and manuscript revision.

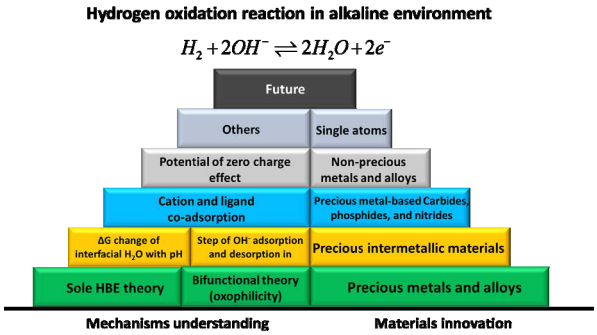

Fig. 7. Pyramidical graph of HOR electrocatalyst development based on reaction mechanism understanding and materials innovation.

Declaration of Competing Interest

The authors declare that they have no known competing financial interests or personal relationships that could have appeared to influence the work reported in this paper.

Electronic supporting information

Supporting information is available in the online version of this article

References

[1] US Department of Energy, The Green Hydrogen Report, NREL, **1995**.
[2] IEA, "*The Future of Hydrogen*." **2019**. Accessed online.
[3] P. E. Dodds, A.Hawkes, Eds., *The Role of Hydrogen andFuel Cells in Providing Affordable, Secure Low-Carbon Heat*. H2FC SUPERGEN, London, UK, **2014**.
[4] B. C. H. Steele, A. Heinzel, *Nature*, **2001**, 414, 345–352.
[5] D. R. Dekel, *J. Power Sources*, **2018**, 375, 158–169.
[6] Y. Qiu, J. J. Huo, F. Jia, B. H. Shanks, W. Z. Li, *J. Mater. Chem. A*, **2016**, 4, 83–95.
[7] Y. Qiu, L. Xin, F. Jia, J. Xie, W. Z. Li, *Langmuir*, **2016**, 32,

Graphical Abstract

Chin. J. Catal., 2021, 42: 2094–2104 doi: 10.1016/S1872-2067(21)64088-3

Electrocatalysts development for hydrogen oxidation reaction in alkaline media: From mechanism understanding to materials design

Yang Qiu, Xiaohong Xie, Wenzhen Li *, Yuyan Shao *
Pacific Northwest National Laboratory, USA; Iowa State University, USA; DOE's Ames Laboratory, USA

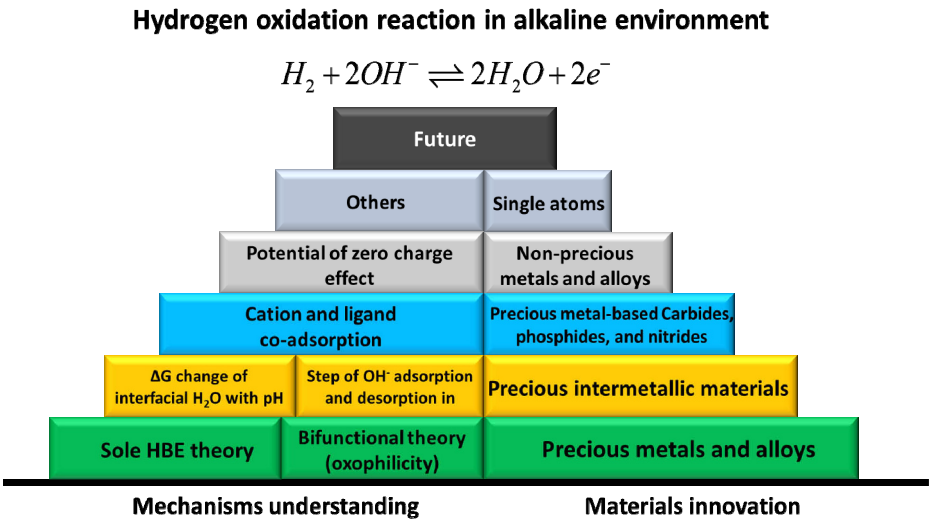

Orders of magnitude slower HOR kinetics in base attracts great attention in cost-effective and highly active electrocatalyst development. This review focuses on recent progress of HOR mechanism understanding and materials innovation in alkaline environment.

12569–12578.
[8] Y. Jiao, Y. Zheng, M. Jaroniec, S. Z. Qiao, *J. Am. Chem. Soc.*, **2014**, 136, 4394–4403.
[9] Y. Li, Q. Li, H. Wang, L. Zhang, D. P. Wilkinson, J. Zhang, *Electrochem. Energy Rev.*, **2019**, 2, 518–538.
[10] Y. He, Q. Tan, L. Lu, J. Sokolowski, G. Wu, *Electrochem. Energy Rev.*, **2019**, 2, 231–251.
[11] C. A. Campos-Roldán, N. Alonso-Vante, *Electrochem. Energy Rev.*, **2019**, 2, 312–331.
[12] N. Ramaswamy, S. Mukerjee, *Chem. Rev.*, **2019**, 119, 11945–11979.
[13] H. A. Firouzjaie, W. E. Mustain, *ACS Catal.*, **2020**, 10, 225–234.
[14] N. M. Markovic, T. J. Schmidt, V. Stamenkovic, P. N. Ross, *Fuel Cells*, **2001**, 1, 105–116.
[15] J. Durst, A. Siebel, C. Simon, F. Hasche, J. Herranz, H. A. Gasteiger, *Energy Environ. Sci.*, **2014**, 7, 2255–2260.
[16] P. J. Rheinlander, J. Herranz, J. Durst, H. A. Gasteiger, *J. Electrochem. Soc.*, **2014**, 161, F1448–F1457.
[17] S. Henning, J. Herranz, H. A. Gasteiger, *J. Electrochem. Soc.*, **2015**, 162, F178–F189.
[18] W. C. Sheng, H. A. Gasteiger, Y. Shao-Horn, *J. Electrochem. Soc.*, **2010**, 157, B1529–B1536.
[19] K. C. Neyerlin, W. B. Gu, J. Jorne, H. A. Gasteiger, *J. Electrochem. Soc.*, **2007**, 154, B631–B635.
[20] J. Durst, C. Simon, F. Hasche, H. A. Gasteiger, *J. Electrochem. Soc.*, **2015**, 162, F190–F203.
[21] W. C. Sheng, M. N. Z. Myint, J. G. G. Chen, Y. S. Yan, *Energy Environ. Sci.*, **2013**, 6, 1509–1512.
[22] W. C. Sheng, Z. B. Zhuang, M. R. Gao, J. Zheng, J. G. G. Chen, Y. S. Yan, *Nat. Commun.*, **2015**, 6, 5848.
[23] W. C. Sheng, A. P. Bivens, M. Myint, Z. B. Zhuang, R. V. Forest, Q. R. Fang, J. G. Chen, Y. S. Yan, *Energy Environ. Sci.*, **2014**, 7, 1719–1724.
[24] S. Trasatti, *J. Electroanal. Chem. Interfacial Electrochem.*, **1972**, 39, 163–184.
[25] J. K. Norskov, T. Bligaard, A. Logadottir, J. R. Kitchin, J. G. Chen, S. Pandelov, J. K. Norskov, *J. Electrochem. Soc.*, **2005**, 152, J23–J26.
[26] E. Skulason, V. Tripkovic, M. E. Bjorketun, S. Gudmundsdottir, G. Karlberg, J. Rossmeisl, T. Bligaard, H. Jonsson, J. K. Norskov, *J. Phys. Chem. C*, **2010**, 114, 18182–18197.
[27] M. J. T. C. van der Niet, N. Garcia-Araez, J. Hernandez, J. M. Feliu, M. T. M. Koper, *Catal. Today*, **2013**, 202, 105–113.
[28] I. Ledezma-Yanez, W. D. Z. Wallace, P. Sebastian-Pascual, V. Climent, J. M. Feliu, M. T. M. Koper, *Nat. Energy*, **2017**, 2, 17031.
[29] I. T. McCrum, M. J. Janik, *J. Phys. Chem. C*, **2016**, 120, 457–471.
[30] X. T. Chen, I. T. McCrum, K. A. Schwarz, M. J. Janik, M. T. M. Koper, *Angew. Chem. Int. Ed.*, **2017**, 56, 15025–15029.
[31] J. Zheng, J. Nash, B. J. Xu, Y. S. Yan, *J. Electrochem. Soc.*, **2018**, 165, H27–H29.
[32] S. A. Giles, J. C. Wilson, J. Nash, B. J. Xu, D. G. Vlachos, Y. S. Yan, *J. Catal.*, **2018**, 367, 328–331.
[33] D. Strmcnik, M. Uchimura, C. Wang, R. Subbaraman, N. Danilovic, D. van der Vliet, A. P. Paulikas, V. R. Stamenkovic, N. M. Markovic, *Nat. Chem.*, **2013**, 5, 300–306.
[34] Y. Wang, G. Wang, G. Li, B. Huang, J. Pan, Q. Liu, J. Han, L. Xiao, J. Lu, L. Zhuang, *Energy Environ. Sci.*, **2015**, 8, 177–181.

[35] J. K. Li, S. Ghoshal, M. K. Bates, T. E. Miller, V. Davies, E. Stavitski, K. Attenkofer, S. Mukerjee, Z. F. Ma, Q. Y. Jia, *Angew. Chem. Int. Ed.*, **2017**, 56, 15594–15598.

[36] Y. Qiu, L. Xin, Y. W. Li, I. T. McCrum, F. M. Guo, T. Ma, Y. Ren, Q. Liu, L. Zhou, S. Gu, M. J. Janik, W. Z. Li, *J. Am. Chem. Soc.*, **2018**, 140, 16580–16588.

[37] I. T. McCrum, M. T. M. Koper, *Nat. Energy*, **2020**, 5, 891–899.

[38] L. Rebollar, S. Intikhab, N. J. Oliveira, Y. Yan, B. Xu, I. T. McCrum, J. D. Snyder, M. H. Tang, *ACS Catal.*, **2020**, 10, 14747–14762.

[39] J. X. Wang, T. E. Springer, R. R. Adzic, *J. Electrochem. Soc.*, **2006**, 153, A1732–A1740.

[40] N. Ramaswamy, S. Ghoshal, M. K. Bates, Q. Y. Jia, J. K. Li, S. Mukerjee, *Nano Energy*, **2017**, 41, 765–771.

[41] E. S. Davydova, S. Mukerjee, F. Jaouen, D. R. Dekel, *ACS Catal.*, **2018**, 8, 6665–6690.

[42] J. X. Wang, S. R. Brankovic, Y. Zhu, J. C. Hanson, R. R. Adzic, *J. Electrochem. Soc.*, **2003**, 150, A1108–A1117.

[43] J. Zheng, Z. B. Zhuang, B. J. Xu, Y. S. Yan, *ACS Catal.*, **2015**, 5, 4449–4455.

[44] J. Zheng, S. Y. Zhou, S. Gu, B. J. Xu, Y. S. Yan, *J. Electrochem. Soc.*, **2016**, 163, F499–F506.

[45] T. Shinagawa, A. T. Garcia-Esparza, K. Takanabe, *Sci Rep.*, **2015**, 5, 13801.

[46] G. Ertl, H. Knozinger, J. Weitkamp, Ed., *Handbook of Heterogeneous Catalysis*, Vol. 8, Wiley-VCH, Weinheim, Germany, **2008**.

[47] X. Y. Tian, P. C. Zhao, W. C. Sheng, *Adv. Mater.*, **2019**, 31, 1808066

[48] Y. Qiu, L. Xin, W. Z. Li, *Langmuir*, **2014**, 30, 7893–7901.

[49] A. J. Bard, L. R. Faulkner, *Electrochemical Methods: Fundamentals and Applications*, John Wiley & Sons Inc., New York, **2001**.

[50] J. K. Norskov, J. Rossmeisl, A. Logadottir, L. Lindqvist, J. R. Kitchin, T. Bligaard, H. Jonsson, *J. Phys. Chem. B*, **2004**, 108, 17886–17892.

[51] P. Quaino, F. Juarez, E. Santos, W. Schmickler, *Beilstein J. Nanotechnol.*, **2014**, 5, 846–854.

[52] J. Greeley, T. F. Jaramillo, J. Bonde, I. B. Chorkendorff, J. K. Norskov, *Nat. Mater.*, **2006**, 5, 909–913.

[53] J. Greeley, J. K. Norskov, L. A. Kibler, A. M. El-Aziz, D. M. Kolb, *ChemPhysChem*, **2006**, 7, 1032–1035.

[54] M. Shao, *J. Power Sources*, **2011**, 196, 2433–2444.

[55] K. Elbert, J. Hu, Z. Ma, Y. Zhang, G. Chen, W. An, P. Liu, H. S. Isaacs, R. R. Adzic, J. X. Wang, *ACS Catal.*, **2015**, 5, 6764–6772.

[56] S. M. Alia, B. S. Pivovar, Y. S. Yan, *J. Am. Chem. Soc.*, **2013**, 135, 13473–13478.

[57] S. M. Alia, Y. S. Yan, *J. Electrochem. Soc.*, **2015**, 162, F849–F853.

[58] M. E. Scofield, Y. C. Zhou, S. Y. Yue, L. Wang, D. Su, X. Tong, M. B. Vukmirovic, R. R. Adzic, S. S. Wong, *ACS Catal.*, **2016**, 6, 3895–3908.

[59] Y. R. Xue, L. Shi, X. R. Liu, J. J. Fang, X. D. Wang, B. P. Setzler, W. Zhu, Y. S. Yan, Z. B. Zhuang, *Nat. Commun.*, **2020**, 11, 5651

[60] S. St John, R. W. Atkinson, R. R. Unocic, T. A. Zawodzinski, A. B. Papandrew, *J. Phys. Chem. C*, **2015**, 119, 13481–13487.

[61] S. M. Alia, B. S. Pivovar, *J. Electrochem. Soc.*, **2018**, 165, F441–F455.

[62] X. P. Qin, L. L. Zhang, G. L. Xu, S. Q. Zhu, Q. Wang, M. Gu, X. Y. Zhang, C. J. Sun, P. B. Balbuena, K. Amine, M. H. Shao, *ACS. Catal.*, **2019**, 9, 9614–9621.

[63] S. Q. Lu, Z. B. Zhuang, *J. Am. Chem. Soc.*, **2017**, 139, 5156–5163.

[64] H. A. Miller, F. Vizza, M. Marelli, A. Zadick, L. Dubau, M. Chatenet, S. Geiger, S. Cherevko, H. Doan, R. K. Pavlicek, S. Mukerjee, D. R. Dekel, *Nano Energy*, **2017**, 33, 293–305.

[65] C. P. Huang, M. C. Tsai, X. M. Wang, H. S. Cheng, Y. H. Mao, C. J. Pan, J. N. Lin, L. D. Tsai, T. S. Chan, W. N. Su, B. J. Hwang, *Catal. Sci. Technol.*, **2020**, 10, 893–903.

[66] Y. Y. Zhou, Z. Y. Xie, J. X. Jiang, J. Wang, X. Y. Song, Q. He, W. Ding, Z. D. Wei, *Nat. Catal.*, **2020**, 3, 454–462.

[67] Z. Zhang, P. Li, Q. Wang, Q. Feng, Y. Tao, J. Xu, C. Jiang, X. Lu, J. Fan, M. Gu, H. Li, H. Wang, *J. Mater. Chem. A*, **2019**, 7, 2780–2786.

[68] S. Drouet, J. Creus, V. Colliere, C. Amiens, J. Garcia-Anton, X. Sala, K. Philippot, *Chem. Commun.*, **2017**, 53, 11713–11716.

[69] H. S. Wang, H. D. Abruna, *J. Am. Chem. Soc.*, **2017**, 139, 6807–6810.

[70] J. Zheng, W. C. Sheng, Z. B. Zhuang, B. J. Xu, Y. S. Yan, *Sci. Adv.*, **2016**, 2, e1501602.

[71] J. Rossmeisl, K. Chan, E. Skulason, M. E. Bjorketun, V. Tripkovic, *Catal. Today*, **2016**, 262, 36–40.

[72] S. Kandoi, P. A. Ferrin, M. Mavrikakis, *Top. Catal.*, **2010**, 53, 384–392.

[73] G. Wu, K. L. More, C. M. Johnston, P. Zelenay, *Science*, **2011**, 332, 443–447.

[74] H. B. Yang, J. W. Miao, S. F. Hung, J. Z. Chen, H. B. Tao, X. Z. Wang, L. P. Zhang, R. Chen, J. J. Gao, H. M. Chen, L. M. Dai, B. Liu, *Sci. Adv.*, **2016**, 2, e1501122.

[75] W. Wei, H. W. Liang, K. Parvez, X. D. Zhuang, X. L. Feng, K. Mullen, *Angew. Chem. Int. Ed.*, **2014**, 53, 1570–1574.

[76] U. A. Paulus, A. Wokaun, G. G. Scherer, T. J. Schmidt, V. Stamenkovic, V. Radmilovic, N. M. Markovic, P. N. Ross, *J. Phys. Chem. B*, **2002**, 106, 4181–4191.

[77] X. X. Wang, D. A. Cullen, Y. T. Pan, S. Hwang, M. Y. Wang, Z. X. Feng, J. Y. Wang, M. H. Engelhard, H. G. Zhang, Y. H. He, Y. Y. Shao, D. Su, K. L. More, J. S. Spendelow, G. Wu, *Adv. Mater.*, **2018**, 30, 1706758.

[78] S. A. Giles, Y. S. Yan, D. G. Vlachos, *ACS Catal.*, **2019**, 9, 1129–1139.

[79] Z. B. Zhuang, S. A. Giles, J. Zheng, G. R. Jenness, S. Caratzoulas, D. G. Vlachos, Y. S. Yan, *Nat. Commun.*, **2016**, 7, 10141.

[80] D. Gao, J. N. Guo, X. Cui, L. Yang, Y. Yang, H. C. He, P. Xiao, Y. H. Zhang, *ACS Appl. Mater. Interfaces*, **2017**, 9, 22420–22431.

[81] F. Z. Song, W. Li, J. Q. Yang, G. Q. Han, P. L. Liao, Y. J. Sun, *Nat. Commun.*, **2018**, 9, 4531.

[82] W. Y. Ni, A. Krammer, C. S. Hsu, H. M. Chen, A. Schuler, X. L. Hu, *Angew. Chem. Int. Ed.*, **2019**, 58, 7445–7449.

[83] F. L. Yang, X. Bao, Y. M. Zhao, X. W. Wang, G. Z. Cheng, W. Luo, *J. Mater. Chem. A*, **2019**, 7, 10936–10941.

[84] Y. F. Gao, H. Q. Peng, Y. M. Wang, G. W. Wang, L. Xiao, J. T. Lu, L. Zhuang, *ACS Appl. Mater. Interfaces*, **2020**, 12, 31575–31581.

[85] O. V. Cherstiouk, P. A. Simonov, A. G. Oshchepkov, V. I. Zaikovskii, T. Y. Kardash, A. Bonnefont, V. N. Parmon, E. R. Savinova, *J. Electroanal. Chem.*, **2016**, 783, 146–151.

[86] L. Gao, Y. Wang, H. Li, Q. Li, N. Ta, L. Zhuang, Q. Fu, X. Bao, *Chem. Sci.*, **2017**, 8, 5728–5734.

[87] S. Kabir, K. Lemire, K. Artyushkova, A. Roy, M. Odgaard, D. Schlueter, A. Oshchepkov, A. Bonnefont, E. Savinova, D. C. Sabarirajan, P. Mandal, E. J. Crumlin, Iryna V. Zenyuk, P. Atanassov, A. Serov, *J. Mater. Chem. A*, **2017**, 5, 24433–24443.

[88] E. S. Davydova, F. D. Speck, M. T. Y. Paul, D. R. Dekel, S. Cherevko, *ACS Catal.*, **2019**, 9, 6837–6845.

[89] Y. Duan, Z. Y. Yu, L. Yang, L. R. Zheng, C. T. Zhang, X. T. Yang, F. Y. Gao, X. L. Zhang, X. X. Yu, R. Liu, H. H. Ding, C. Gu, X. S. Zheng, L. Shi, J. Jiang, J. F. Zhu, M. R. Gao, S. H. Yu, *Nat. Commun.*, **2020**, 11, 4789.

[90] M. Wang, H. Yang, J. N. Shi, Y. F. Chen, Y. Zhou, L. G. Wang, S. J. Di, X. Zhao, J. Zhong, T. Cheng, W. Zhou, Y. G. Li, *Angew. Chem. Int. Ed*, **2021**, 60, 5771–5777.

[91] A. G. Oshchepkov, P. A. Simonov, O. V. Cherstiouk, R. R. Nazmutdinov, D. V. Glukhov, V. I. Zaikovskii, T. Y. Kardash, R. I. Kvon, A. Bonnefont, A. N. Simonov, V. N. Parmon, E. R. Savinova, *Top. Catal.*, **2015**, 58, 1181–1192.

[92] J. Ohyama, T. Sato, Y. Yamamoto, S. Arai, A. Satsuma, *J. Am. Chem. Soc.*, **2013**, 135, 8016–8021.

[93] T. Zhao, G. Wang, M. Gong, D. Xiao, Y. Chen, T. Shen, Y. Lu, J. Zhang,

H. Xin, Q. Li, D. Wang, *ACS Catal.*, **2020**, 10, 15207–15216.
[94] A. F. Innocente, A. C. D. Ângelo, *J. Power Sources*, **2006**, 162, 151–159.
[95] L. Rößner, M. Armbrüster, *ACS Catal.*, **2019**, 9, 2018–2062.

碱性介质中氢氧化反应电催化剂的开发：从机理认识到材料设计

仇暘[a], 谢小红[a], 李文震[b,c,#], 邵玉艳[a,*]
[a]西北太平洋国家实验室, 华盛顿, 美国
[b]爱荷华州立大学化学与生物工程系, 爱荷华州, 美国
[c]能源部艾姆斯实验室, 爱荷华州, 美国

摘要: 阴离子交换膜(AEM)燃料电池因具有使用非贵金属作为催化剂的优点而受到广泛关注. 然而, 在碱性体系中, AEM燃料电池中氢氧化反应(HOR)的反应动力学比在酸性介质中的慢两个数量级. 针对HOR在碱中动力学缓慢的问题, 有两种主要的理论来解释, (1)pH相关的氢结合能作为主要影响因素来控制HOR动力学的理论; (2) 质子和氢氧根离子的吸附共同作为影响因子来控制HOR在碱性条件下的动力学的双功能理论.

本文首先讨论了在碱性电解质中可能的HOR反应机理及其Tafel性能变化. 除了传统的Tafel-Volmer和Heyrovsky-Volmer-HOR机理外, 还讨论了最新提出的氢氧根离子吸附参与的HOR机理来说明在酸性和碱性介质中HOR机理的差异. 然后, 总结了具有代表性的碱性HOR催化剂(如贵金属、合金、金属间化合物、镍基合金、碳化物、氮化物等), 简要介绍了它们相应的HOR反应机理, 从而进一步理解在碱性介质中不同基元反应步骤给HOR性能带来的差异. 最后, 提出了一种未来设计HOR碱性催化剂的可行性方案, 为今后碱性环境下的HOR催化剂设计提供参考.

关键词: 氢氧化反应; 碱性电解质; 燃料电池; 电催化剂; 电催化; 氢和氢氧离子结合能

收稿日期: 2021-01-18. 接受日期: 2021-04-07. 上网时间: 2021-09-10.
*通讯联系人. 电子信箱: yuyan.shao@pnnl.gov
#通讯联系人. 电子信箱: wzli@iastate.edu
本文的电子版全文由Elsevier出版社在ScienceDirect上出版(http://www.sciencedirect.com/journal/chinese-journal-of-catalysis).